Cryogenics 126 (2022) 103523

Contents lists available at ScienceDirect

Cryogenics

journal homepage: www.elsevier.com/locate/cryogenics

Effects of bending and torsion behavior on I_c degradation and microstructure of ReBCO coated conductors

Xianhao Li, Zili Yang, Ying Xu, Li Ren *, Haipeng Zhang, Xuan Ding, Yuejin Tang

State Key Laboratory of Advanced Electromagnetic Engineering and Technology, Wuhan 430074, China
School of Electrical and Electronic Engineering, Huazhong University of Science and Technology, Wuhan 430074, China

ARTICLE INFO

Keywords:
Critical current
Performance degradation
Bending and torsion
Microstructure
Crack

ABSTRACT

The performance degradation caused by bending and torsion is crucial for the application of superconducting coated conductors. In this study, we investigated the critical current (I_c) degradation of four kinds of conductors under bending and torsion. With 1 mm resolution, the critical bending radius of STT236μm (Shanghai Superconductor Technology) conductors is 6–7 mm, and that of STT380μm conductors is 4–5 mm, and that of SAMRI (Suzhou Advanced Materials Research Institute) conductors is 4 mm. With better bending tolerance, SAMRI conductors also have a less critical twist pitch of 82–87 mm. Considering the residual thermal stress during fabrication, the longitudinal strain corresponding to 5 % I_c degradation is 0.484 %. Further, to figure out the failure mechanism of coated conductors, the micromorphology of the ReBCO layer was observed after chemical etching. The crack distribution not only verified the cause of I_c degradation under mechanical behaviors, but also helps to develop a crack-based I_c prediction method.

1. Introduction

ReBCO coated conductors, composed of multiple laminated layers, are more robust than the first-generation (1G) high temperature superconducting (HTS) wires [1–2]. Superconducting cables, composed of multiple conductors in a strand, are widely used in superconducting applications. Compared to the tensile tolerance up to 500 MPa [3], the bending and torsion behavior is more crucial to the performance of superconducting cables. Since these mechanical behaviors are inevitable, for example, TSTC (twisted stacked tape cable) cable eliminates anisotropy by torsion, and CORC (conductor on round core) cable winds coils or avoids roadblocks by bending, the critical parameters and failure mechanism of conductors should be investigated.

Many studies have reported the measurement of I_c under bending and torsion, and calculated the strain-dependent I_c with different materials [4–8]. However, most of them were aimed at widely-used commercial ReBCO tapes, such as the SCS4050 tape of SuperPower Inc. For HTS power cables, coated conductors with a customized thick stabilizing layer are preferred for their high over-current capacity [9], which may withstand short-circuit faults in the distribution network. Besides, with the improvement of wire production technology in China, there are blanks about their fundamental mechanical properties. Therefore, the main test objects of this work are thick coated conductors. As for the corresponding critical strain of the ReBCO layer, the more feasible method to determine is to calculate it numerically, since it is in the inner of the conductor. Even though the effect of intrinsic strain on conductor properties has long been confirmed by experiments, it is only in recent years that the residual thermal stress (RTS) accumulated during fabrication has been calculated numerically [10]. Therefore, the effect of strain on I_c should be corrected with refined finite element models. Most importantly, the prediction of I_c is generally based on the result of the uniaxial tensile test [4,11–12]. However, bending and torsion have different behaviors and damage modes from uniaxial tensile [10,13]. To estimate the I_c under complex mechanical behavior, the prediction should be based on the failure mechanism of coated conductors, which can be observed and developed by micromorphology.

In response to these problems, a series of experiments were carried out to investigate the effect of bending and torsion behavior on conductor properties. The I_c degradation curves of four types of conductors were measured. Combined with the simulation results, longitudinal strains that conductors can bear were given. To determine the causes of the I_c degradation, chemical etching and ESEM (environmental scanning electro microscope) were introduced to observe the micromorphology of the ReBCO layer. This work gives the critical strain of

* Corresponding author.
E-mail address: renli@mail.hust.edu.cn (L. Ren).

https://doi.org/10.1016/j.cryogenics.2022.103523
Received 23 January 2022; Received in revised form 6 June 2022; Accepted 12 July 2022
Available online 19 July 2022
0011-2275/© 2022 Published by Elsevier Ltd.

thick coated conductors, which can be used as a criterion for the subsequent calculation of HTS cables' critical bending radius [14]. The ESEM results reflect the failure mechanism of coated conductors under bending and torsion for the first time, which can contribute to developing new I_c prediction methods based on the crack growth mode.

2. Experimental setup

2.1. Tested conductors

We investigated four types of ReBCO conductors, two from Shanghai Superconductors Technology (STT), and two from Suzhou Advanced Materials Research Institute (SAMRI). The specifications of these conductors are given in Table 1. The main difference between the two Chinese companies is the ReBCO layer growth method. STT conductors use pulsed laser deposition (PLD), and SAMRI conductors adopt metal–organic chemical vapor deposition (MOCVD) as SuperPower Inc. In addition, the difference in conductor parameters mainly comes from the copper stabilizer layer on both sides. For convenience, we use the company abbreviation plus conductor thickness, such as STT236um, to represent these four conductors.

2.2. I_c measurement under bending

The bending device for I_c measurement is shown in Fig. 1. With an epoxy plate as a framework, the test device is mainly composed of copper sliding rods and glass fiber reinforced plastics (GFRP) cylinders. To measure the I_c under bending, the tested sample is closely attached to the cylindrical surface and fixed to copper sliding rods. Current is powered by copper sliding rods that are connected with current leads, and the bending radius of the sample is equal to the outer radius of the cylinder. Ignoring cryogenic shrinkage of GFRP cylinders with a low coefficient of thermal expansion, the test radius of the bending device ranges from 60 mm to 3 mm. As cylinders with different radii locate at different heights, sliding rods are helpful to keep the sample position horizontal.

Before bending, we used the four-probe method to measure the sample's initial critical current (I_{c0}). Then, the middle part of the sample was bent on the bottom cylinder surface. Considering the residual thermal stress during fabrication, the tensile behavior on the ReBCO layer has a greater influence on I_c degradation than compression behavior [4,14]. Therefore, the ReBCO layer was stretched on the outside in each test to obtain its limit characteristics. After the I_c was measured, the sample was bent on a cylinder with a smaller radius. The test continued until the I_c was less than 95 % I_{c0}, which is recognized as irreversible, or the sample was burned down.

2.3. I_c measurement under torsion

The torsion device for I_c measurement is shown in Fig. 2. Two 300 mm long copper rods were used as supports to prevent deformation of the sample holder. One end of the conductor holder was connected to a current lead and completely fixed; the other end of the conductor holder was connected to another current lead but can rotate. According to the dial marked on the plate, the twist pitch can be easily calculated. Controlled by a continuous torsion angle, the torsion test device has a higher resolution, which is helpful to obtain a strain-dependent I_c degradation curve.

Similar to the bending test procedure, the I_{c0} of the sample was first measured before twisting. Then, the holder was rotated to drive the conductor to twist and the I_c of the sample was remeasured. Because the torsion behavior is symmetrical in the width and thickness directions [15], it is not necessary to focus on the conductor's front and back surfaces like bending. With the torsion angle increasing, the test continued until the I_c was less than 95 % I_{c0}, or the sample was burned down.

All the above measurements were carried out at 77 K and self-field. An EA EL 9080-340B type DC power supply was used to provide direct current, which was controlled to raise at 0.5 A/s until the sample quenched. The voltage was measured by a Keithley 3706A nanovoltmeters, and the quench criterion of 0.1 μV/cm was used to monitor the voltage measurement area.

2.4. Microstructure scanning after etching

Since the ReBCO layer is inside the coated conductor, conventional

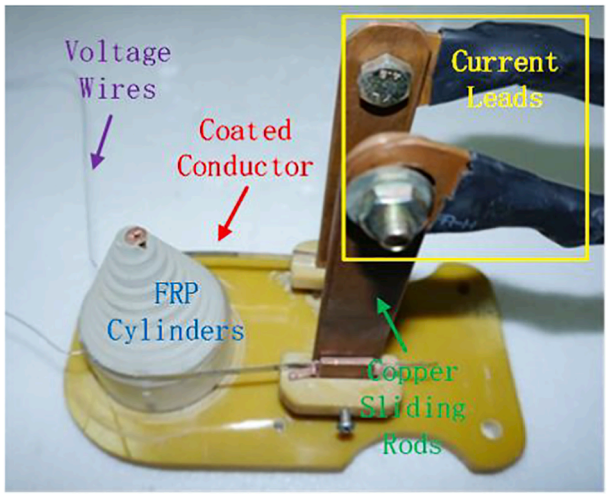

Fig. 1. Picture of the bending test device.

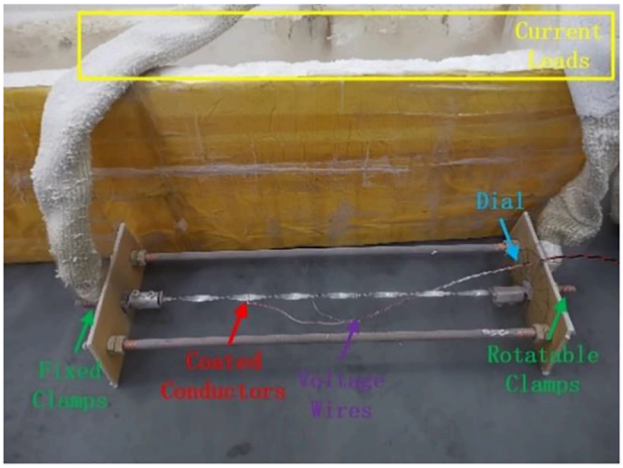

Fig. 2. Picture of the torsion test device.

Table 1
Specifications of four types of ReBCO conductors.

Item	STT		SAMRI	
Thickness of ReBCO layer/μm	2		0.7	
Thickness of buffer layer/μm	0.325		0.2	
Thickness of silver layer/μm	1.5		1.7 (on both surfaces)	
Thickness of substrate layer/μm	50		61	
Thickness of copper layer/μm	5		3.8	
Thickness of stabilizer layer per surface/μm	85	160	60	120
Total thickness of conductor/μm	~236	~380	~180	~316
Width of ReBCO layer/mm	4		4	
Width of conductor/mm	4.8		5	
Critical current/A @77 K, self field	207	203	106	>135

detection techniques, such as ultrasonic scanning, are difficult to accurately describe the appearance of the ReBCO layer. Therefore, the chemical etching method was adopted to remove the outer layers of the ReBCO layer. According to the stacking order of the coated conductor, it was etched layer by layer in the following steps:

First, sandpaper was used to slowly grind off the tin plating on the outermost layer. Then, the conductor was immersed in diluted nitric acid [16]. Without tin plating, the copper stabilizer can fully react with nitric acid. The sample was taken out when its surface turned white, which means the copper was removed. Next, the processed conductor without a copper stabilizer layer was immersed in a mixture of ammonia to etch its silver layer [17–18]. Several minutes later, a complete ReBCO layer was obtained, which appeared as bright black over the conductor surface.

As the mechanical damage can be directly detected after chemical etching, ESEM, which is widely used in material science and life science, was chosen to observe the micromorphology of the ReBCO layer. Compared with other scanning electro microscope (SEM), ESEM is more convenient to work in ambient vacuum mode. The Quanta 200 model ESEM was used in the experiment. Produced by FEI company, Netherlands, the ESEM has a resolution of up to 3 nm in ambient vacuum mode. Combined with energy dispersive analysis X-ray (EDAX), the platform can analyze the element composition and determine the scanned ply material.

3. Simulation step

3.1. RTS model

Based on the fabrication process concluded in [10], the residual thermal stress of coated conductors was modeled in COMSOL Multiphysics as follows: According to the specification parameters listed in Table 1 and material parameters in [11], a long-straight 3D geometric part was built to represent the tape. In the first step, the domain of the ReBCO layer was activated to simulate its fabrication process, and the thermal expansion function was used to calculate the annealing process from ~ 1000 K to 770 K. Then, the domain of the stabilizer layer was activated to simulate the electroplating process, and the annealing process was calculated from 770 K to room temperature or cryogenic temperature.

As the stacking structure of coated conductors is not symmetric in the thickness direction, the bottom surface of the substrate layer was only allowed to deform in the longitudinal and width directions, which can prevent the part from bending during cooling. Besides, the silver layer and side stabilizer layer were ignored in the model, since their small stiffness and volume ratio had little effect on the stress distribution of other constituent layers [11].

3.2. Dynamic model

Based on the RTS model, dynamic models with pre-stress loaded were built to compute strain precisely.

For the bending behavior, one end of the conductor was set as a symmetric boundary condition to reduce the calculation, and the bottom of the conductor was moved by the prescribed displacement boundary condition to ensure the bending radius was consistent. According to the geometric relationship, the displacement of the surface can be given by the following equation:

$$\begin{bmatrix} u_1 \\ u_2 \\ u_3 \end{bmatrix} = \begin{bmatrix} -\left(x - R\sin(\frac{x}{R})\right) \\ 0 \\ -R\left(1 - \cos(\frac{x}{R})\right) \end{bmatrix} \quad (1)$$

where, u_1, u_2, and u_3 are displacements in the longitudinal direction, width direction, and thickness direction, respectively. x is the coordinate in the length direction, and R is the desired bending radius.

For the torsion behavior, one end of the conductor was completely fixed, and the other end of the conductor was set to rotate. With an additional cylindrical coordinate system established in the rectangular coordinate system, the prescribed displacement was applied in the circumferential direction to control the torsion angle. Besides, the distance between the four rotational vertices can be controlled by global constraints, so that the rotation end and the fixed end have the same surface deformation constraint.

In conclusion, the schematic diagram of the whole simulation process is shown in Fig. 3. The stationary solver was used to decrease the amount of calculation, and the auxiliary sweep technology was used to improve the convergence.

4. Results and discussion

4.1. Bending test results

With more than six samples for each type of conductor, the normalized critical current (I_c/I_{c0}) under different bending radii is shown in Fig. 4. Test results were fitted by exponential function in multi-data concatenate fit mode, and 95 % confidence bands were marked in the figures. In addition, standard deviation (SE) was used to better analyze the test error.

For STT236μm conductors, one sample had 18.62 % I_c degradation at a bending radius of 30 mm, which can be regarded as unreliable data. Two samples were irreversible at the bending radius of 6–7 mm. And two samples' I_c decayed exceeded 50 % at a bending radius of 5 mm. Considering the resolution of the test device, the critical bending radius of STT236μm conductors is 6–7 mm. At this time, the standard deviation is less than 0.14. These conclusions are consistent with the tested results of STT conductors with the ReBCO layer stretched under bending [13]. For STT380μm conductors, four samples had more than 10 % I_c degradation at a bending radius of 5 mm, and one sample's I_c declines even at a bending radius of 3 mm. Within the maximum standard deviation of 0.13, the critical bending radius of STT380μm conductors is 4–5 mm. For SAMRI180μm conductors, all samples were irreversible at a bending radius of 4 mm, and the maximum standard deviation is less than 0.048. Therefore, it can be sure that the critical bending radius of SAMRI180μm conductors is 4 mm. For SAMRI316μm conductors, except that one sample was burned down at a bending radius of 10 mm, the I_c of other samples declined by more than 25 % at a bending radius of 4 mm.

In conclusion, SAMRI conductors have better bending tolerance and consistency than STT conductors, and a thick copper stabilizer layer is conducive to improving the bending performance. Even if the test results are successfully fitted with the exponential function, the I_c of more than 70 % of samples declines by more than 10 % in one increment step, and that of more than 50 % of samples declines by more than 20 % in one increment step, which means the degradation of tape properties caused by bending is rapid and severe.

4.2. Torsion test results

With more than three samples for each type of conductor, the normalized critical current (I_c/I_{c0}) under different torsion angles is shown in Fig. 5. Similarly, the standard deviation was used to analyze the test error. To better illustrate the test results of torsion, the torsion angle was converted to the twist pitch by the following equation:

$$L_p = \frac{L}{\theta/360^\circ} \quad (2)$$

where L/mm is the length of the sample, which is 300 mm in the test. And $\theta/^\circ$ is the torsion angle.

Test results of STT236μm conductors are shown in Fig. 5(a). As

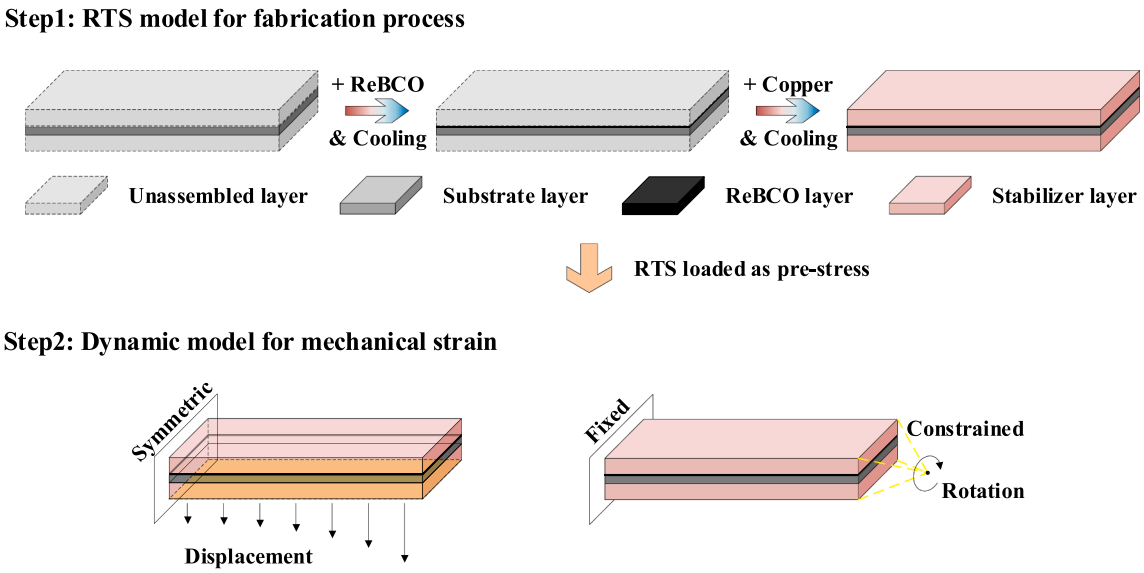

Fig. 3. Schematic diagrams of finite element (FE) models (not to scale).

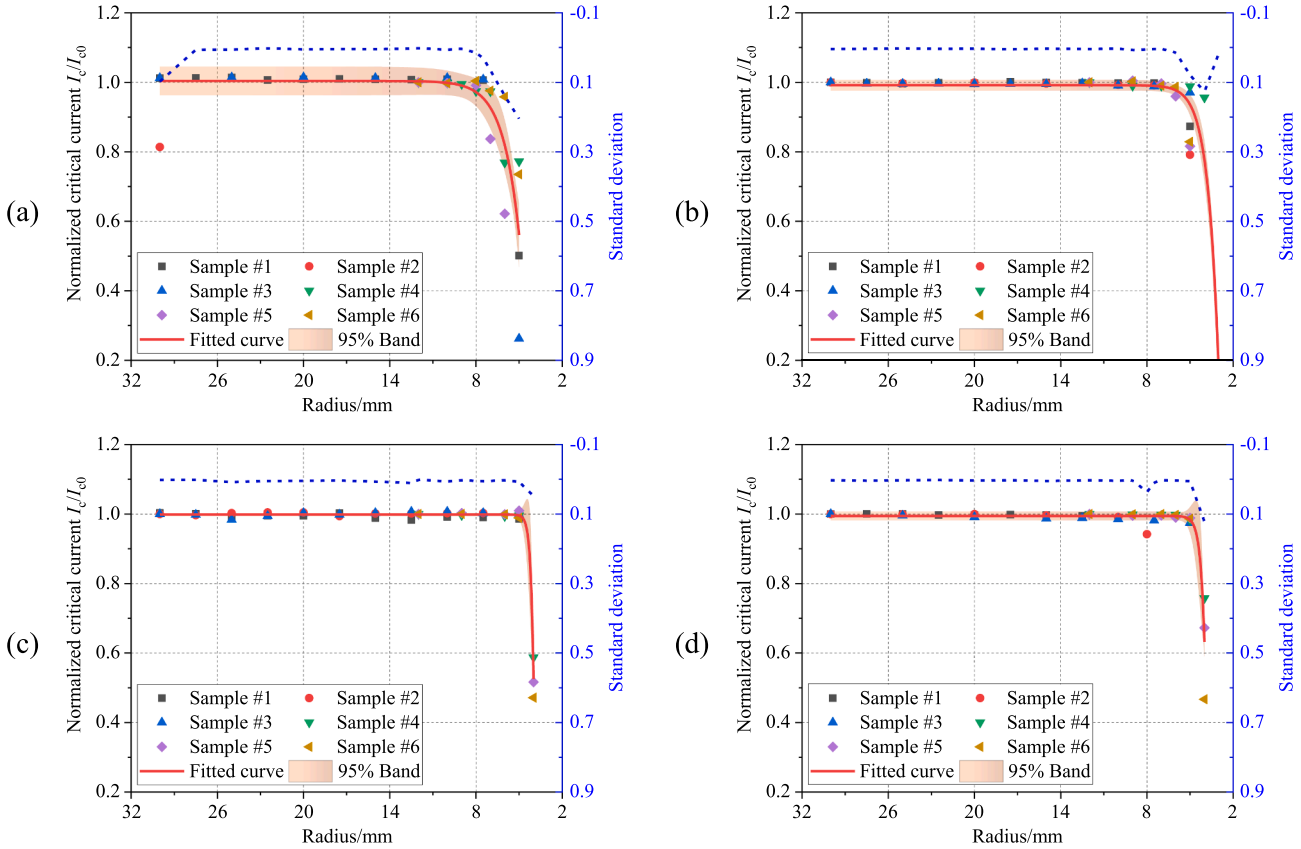

Fig. 4. I_c/I_{c0} of four types of conductors with different bending radii. (a) Test results of STT236μm conductors. (b) Test results of STT380μm conductors. (c) Test results of SAMRI180μm conductors. (d) Test results of SAMRI316μm conductors.

mentioned above, the torsion test device has a better resolution than the bending test device. The exponential function well fits the I_c degradation under different twist pitches. Even though the test results between 99 % and 95 % I_{c0} are as uneven as the bending results, the critical twist pitch of STT236μm conductors can be limited to 100–90 mm under the maximum standard deviation of 0.025.

Test results of STT380μm conductors are shown in Fig. 5(b). Starting from the twist pitch of 300 mm, some samples' I_c decreased significantly. With a thicker copper stabilizer layer, the STT380um conductor has greater dispersion under torsion. The critical twist pitch of 250–300 mm is about 3 times that of STT236μm conductors, and the maximum standard deviation also increased by 8 times. It is worth noticing that slight tensile can increase the conductor's I_c by offsetting the compressive stress accumulated during the fabrication process [4,11]. Since the conductor also experienced tension when it was twisted, this phenomenon also appeared in the torsion behavior.

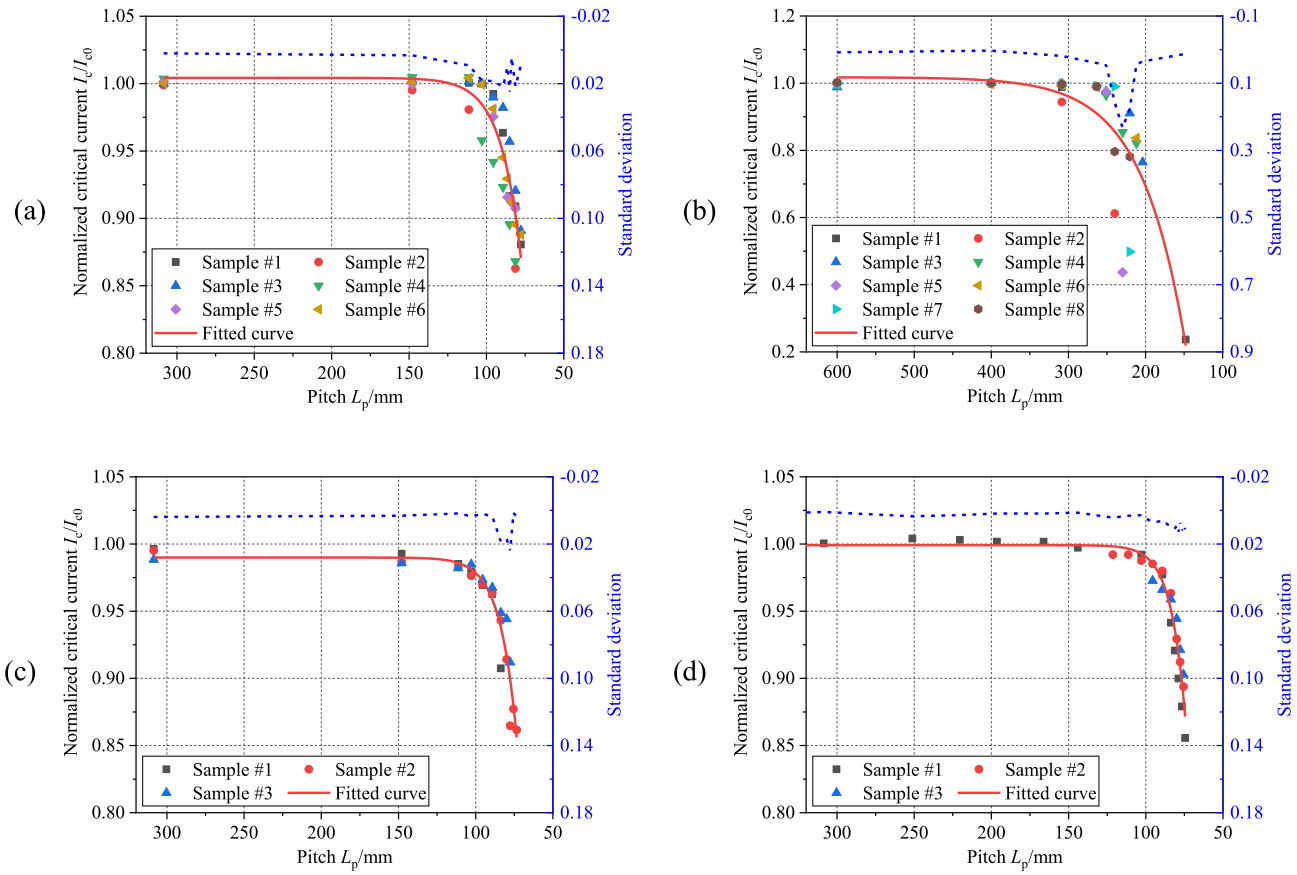

Fig. 5. I_c/I_{c0} of four types of conductors with different torsion angles. (a) Test results of STT236μm conductors. (b) Test results of STT380μm conductors. (c) Test results of SAMRI180μm conductors. (d) Test results of SAMRI316μm conductors.

Test results of SAMRI conductors are shown in Fig. 5(c) and (d). The phenomenon of increasing I_c described above can be seen in Fig. 5(d). Compared with STT conductors, SAMRI conductors show better stability and uniformity for their maximum standard deviation is less than 0.02, or even less than 0.01. The I_c begins to decrease at the twist pitch of 150 mm, and the critical twist pitch corresponding to 95 % I_{c0} is about 85–80 mm. According to fitted curves, the I_c degradation of the two types of conductors under torsion is almost the same, while the one with a thicker copper stabilizer layer has a faster I_c degradation.

In conclusion, twist pitches corresponding to different degrees of I_c degradation are shown in Table 2. The values in brackets are the range of each sample's test results, and the bold ones are the results of curve fitting. Almost all the calculated values of fitting curves fall well within the measurement intervals, especially the results corresponding to the irreversible criterion of 95 % I_{c0}. Except for the STT380μm conductor with the worst torsional tolerance, the other three conductors' twist pitch range corresponding to 99 %~ 95 % I_{c0} is about 20 mm. Among them, the STT236μm conductor has the smallest initial degradation twist pitch and the fastest decay speed. Its critical twist pitch is 90.2 mm and the uncertainty is the largest. For the SAMRI180μm conductor, even though its normalized I_c is less than 1 at the twist pitch of 300 mm, its I_c decreases by 1 % at the twist pitch of 108.1 mm and 5 % at the twist pitch of 86.4 mm. Besides, the SAMRI316μm conductor has the best torsional tolerance performance and a minimum twist pitch of 82.3 mm.

Table 2
Twist pitches of four types of ReBCO conductors under torsion.

Item	STT		SAMRI	
	236 μm	380 μm	180 μm	316 μm
I_c/I_{c0} < 1	~120 mm	~360 mm ~ 300 mm	<300 mm	~150 mm
I_c/I_{c0} < 0.99	**112 mm** (~110 mm ~ 96 mm)	**320 mm** (~360 mm ~ 300 mm)	**108.1 mm** (~135 mm ~ 110 mm)	**102.3 mm** (~110 mm ~ 100 mm)
I_c/I_{c0} < 0.95	**90.2 mm** (~100 mm ~ 85 mm)	**255.9 mm** (~300 mm ~ 240 mm)	**86.4 mm** (~88 mm ~ 84 mm)	**82.3 mm** (~84 mm ~ 82 mm)

4.3. Simulation results

There are few reports on the critical properties of these four types of conductors. Considering the effect of residual thermal stresses, longitudinal strains under mechanical behavior were computed to help estimate their I_c.

Based on the RTS model described in Section 3.1, the residual

Table 3
Residual thermal stress of different ReBCO conductors @77 K.

Item	SuperPower SCS4050		STT		SAMRI	
	Reported in [11]	RTS model	236 μm	380 μm	180 μm	316 μm
Hastelloy substrate layer/ MPa	−55	−54.3	−110.7	−141.5	−94	−133.7
ReBCO layer/ MPa	−648	−648.4	−702.1	−730.2	−686.8	−723.1
Copper stabilizer layer/ MPa	88	87.9	42.5	29.2	55.9	38.7

thermal stresses of each constituent layer are concluded in Table 3. The RTS model was verified by the widely used SCS4050 conductor, produced by SuperPower Inc [19]. Considering the temperature-dependent material properties, the maximum residual thermal stress error is less than 0.5 MPa. Ignoring the influence of constituent layers with small volume fractions, the greater the thickness of the copper stabilizer layer, the greater the stress of the Hastelloy substrate layer and the ReBCO layer.

With the residual thermal stress loaded as pre-stress to the subsequent dynamic model, the longitudinal strain of the ReBCO layer under torsion can be calculated for its better consistency in the test. Based on the results in Table 2, the corresponding longitudinal strains are listed in Table 4.

Similarly, the values in brackets are the range of each sample's test results, and the bold ones are the results of curve fitting. To provide as accurate results as possible, STT380μm conductors with high dispersion were not concluded. Different from the commonly used failure criterion of 0.45 % strain, STT236μm conductors fail at 0.468 % strain. The I_c of SAMRI conductors decreases by 1 % at 0.43 % strain and 5 % at 0.484 % strain.

4.4. ESEM scanning results

To better estimate the I_c, we need to figure out the failure mechanism of coated conductors under bending and torsion. Based on the results of 2D residual magnetic field scanning [20], the microstructure will be investigated to verify the reflected defects. Through the chemical etching and micro-scanning technologies introduced above, two representative samples were tested: 1) STT236μm sample with a bending radius of 5 mm. According to [20], the bending sample may have transverse defects. 2) SAMRI316μm sample with a bending radius of 5 mm, which can be used for comparison since its I_c was not decayed. 3) SAMRI316μm sample with a twist pitch of 74.5 mm. According to the simulation result in Section 4.3, there may be defects on both sides of the conductor.

The pictures of the three samples are shown in Fig. 6. After chemical etching, bent and twisted samples were rebounded into straight tapes. In Fig. 6 (a), the shorter one is the STT236μm sample, and the longer one is the SAMRI316μm sample. Besides, the black part on the conductor is the ReBCO layer mentioned above, and the white part is the unetched constituent layer.

According to the test results in Fig. 4, the I_c of bent samples declines rapidly around the critical bending radius. As a kind of mechanical behavior, it can be considered that this phenomenon is caused by the consistent stress and strain in the width direction of the conductor, and there may be deviation due to small defects produced in fabrication. To verify the above guess, the micro topographies of bending samples are shown in Fig. 7.

There are many transverse cracks in the middle of the sample, where the bending condition is the most serious. Since the current is mainly along the longitudinal direction of the conductor, the transverse crack will block the current flow. As the mechanical behavior is uniform in the width direction under bending, the crack shown in Fig. 7 penetrates the conductor surface macroscopically, which significantly reduces the I_c of the superconducting tape. Besides, it can be seen that there are some precipitated copper particles that appear white. As local weaknesses, they affect the generation of transverse cracks and make them slightly inclined, which may lead to the irregular degradation of I_c. As a comparison, the ReBCO layer of SAMRI316μm sample without I_c degradation is very complete and clean.

Table 4
Longitudinal strain of three ReBCO conductors under torsion.

Item	STT	SAMRI	
	236 μm	180 μm	316 μm
$I_c/I_{c0} <$ 0.99	**0.411 %** (~0.4165 ~ 0.453 %)	**0.429 %** (~0.36 ~ 0.424 %)	**0.431 %** (~0.411 ~ 0.437 %)
$I_c/I_{c0} <$ 0.95	**0.4675 %** (~0.442 ~ 0.481 %)	**0.4841 %** (~0.48 ~ 0.49 %)	**0.4838 %** (~0.479 ~ 0.4846 %)

According to the test results in Fig. 5, the I_c of torsional samples declines gradually with the increase of torsion angle. Based on the analysis of bending behavior, the degradation of I_c under torsional behavior may also be caused by cracks. Combined with the simulation results in Section 4.3, cracks may gradually develop inward from both sides. To confirm the suspicion, the micro topographies of the torsion sample are shown in Fig. 8.

Along the direction of torsion, there are many oblique cracks on both sides of the sample. These cracks show the characteristics of a large root and small top, indicating an inward development process. On the contrary, there is no damage in the middle part of the conductor. This result is consistent with the distribution law of strain in the width direction and the distribution characteristics of residual magnetic field under torsion [20–21].

Combined with the I_c measurement and residual magnetic field scanning results, it can be concluded that: Cracks cuased by mechanical behaviors block the transmission of current, leading to the failure of superconducting conductors. Specifically, the bending behavior is accompanied by penetrating transverse cracks, at which time the I_c decays rapidly; the torsion behavior will generate inward oblique cracks, at which time the degradation of I_c conforms to the strain-dependent exponential mode. The scanning results not only help to observe the failure mechanism of the conductor, but also are conducive to developing a new I_c prediction method. With more material properties measured, the extended finite element method (XFEM) can be introduced to simulate the initiation and development of conductor cracks. Combined with the research on the distribution law of current density, the I_c under mechanical behaviors can be estimated more precisely.

5. Conclusion

Bending and torsion effects of four types of ReBCO conductors were investigated at 77 K and self-field. The critical bending radius of STT236μm conductors is 6–7 mm, and that of STT380μm conductors is 4–5 mm. Fabricated by MOCVD, SAMRI conductors have a better bending tolerance and their critical bending radius is 4 mm. Different from the bending behavior, STT conductors with a thick copper stabilizer layer have a larger dispersion under torsion, and the critical twist pitch of STT236μm conductors is 90 mm. Considering the residual thermal stress during fabrication, the I_c of SAMRI conductors decays 1 % under 0.43 % longitudinal strain, and decays 5 % under 0.483 % longitudinal strain.

In addition, by scanning the ReBCO layer micro topography, it's confirmed that transverse cracks caused by bending, and oblique cracks caused by torsion lead to the I_c degradation. The chemical etching and scanning technology provides a method for detecting the mechanical damage of coated conductors, and the crack micro-morphology provides an experimental reference for thermodynamic damage simulation. More I_c prediction studies can be carried out based on the test results and the failure mechanism.

CRediT authorship contribution statement

Xianhao Li: Conceptualization, Methodology, Software, Formal analysis. **Zili Yang:** Methodology, Validation. **Ying Xu:** Conceptualization. **Li Ren:** Formal analysis, Supervision, Project administration. **Haipeng Zhang:** Validation. **Xuan Ding:** Software, Validation. **Yuejin Tang:** Supervision, Project administration.

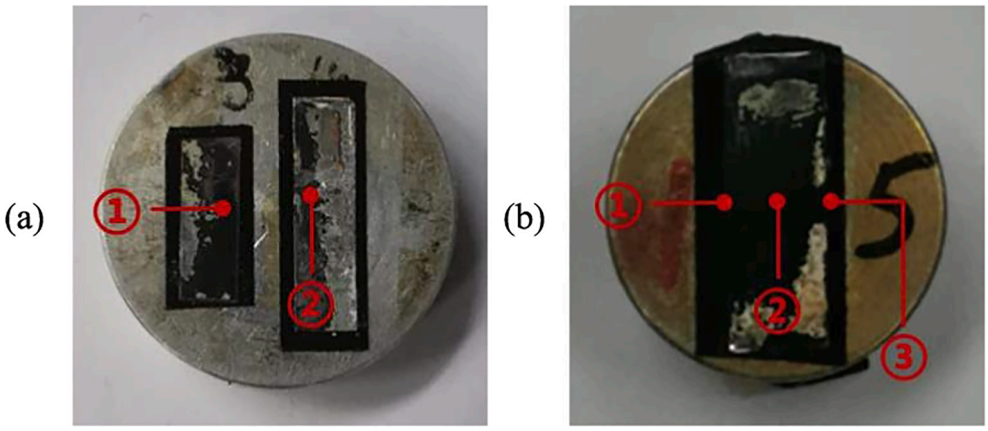

Fig. 6. Three short samples for ESEM scanning. (a) STT236μm and SAMRI316μm after bending. (c) SAMRI316μm after torsion.

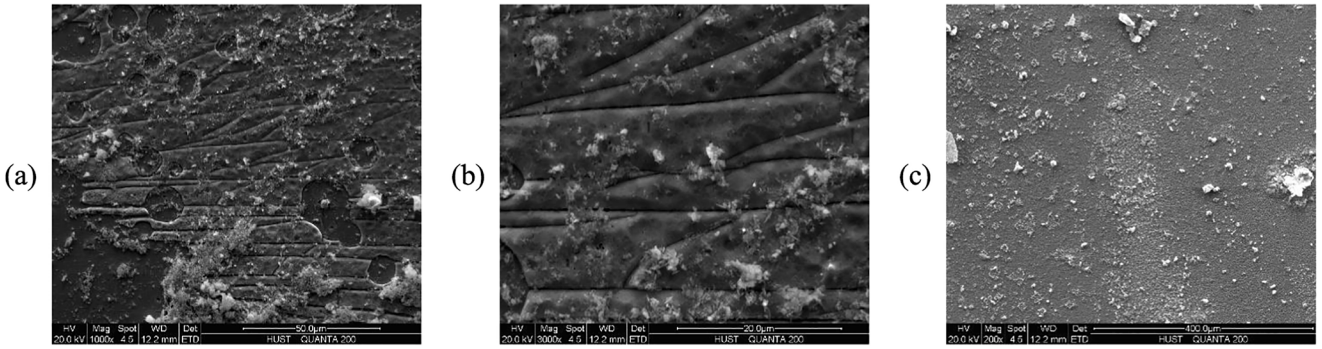

Fig. 7. Scan results of bending samples. (a) Zoom in 1000 times at point #1. (b) Zoom in 3000 times at point #1. (c) Zoom in 200 times at point #2.

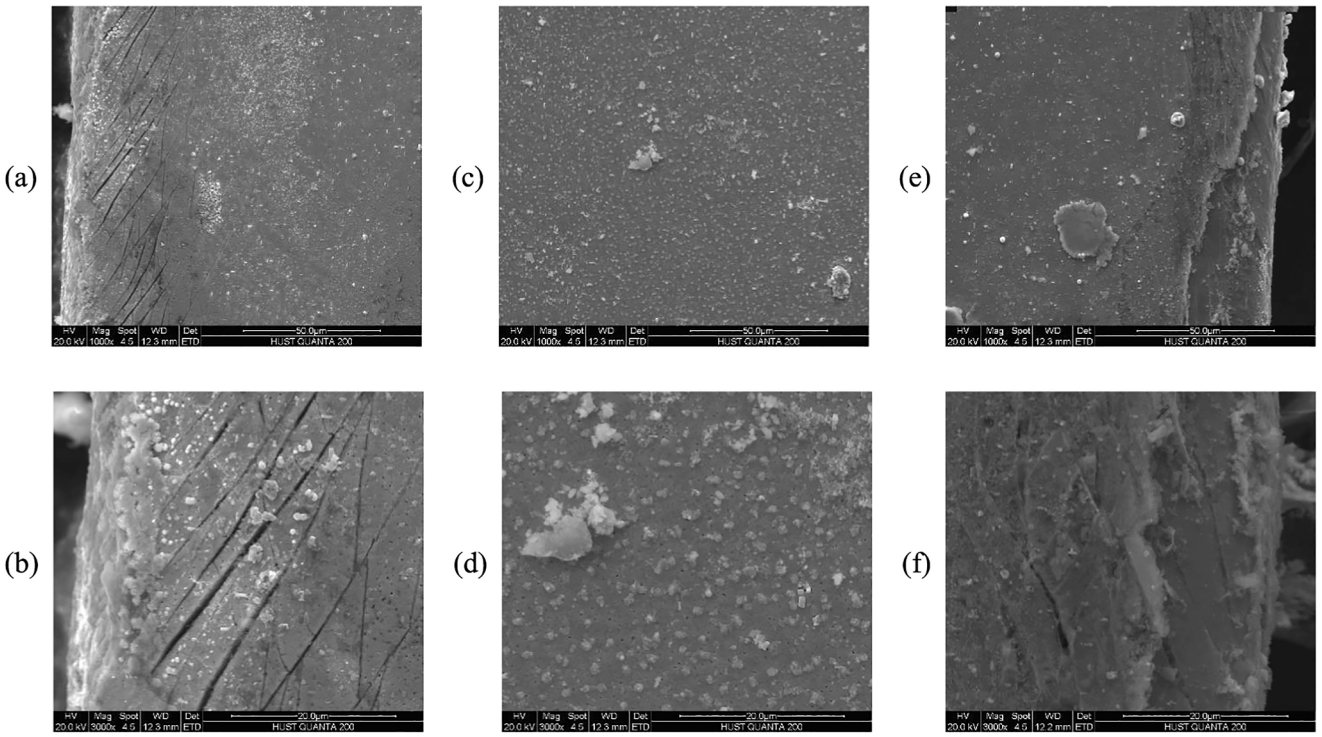

Fig. 8. Scan results of the torsion sample. (a) Zoom in 1000 times at point #1. (c) Zoom in 1000 times at point #2. (e) Zoom in 1000 times at point #3. (b) Zoom in 3000 times at point #1. (d) Zoom in 3000 times at point #2. (f) Zoom in 3000 times at point #3.

Declaration of Competing Interest

The authors declare that they have no known competing financial interests or personal relationships that could have appeared to influence the work reported in this paper.

Acknowledgement

We thank the Analytical and Testing Center of Huazhong University of Science and Technology for providing an ESEM to scan the samples.

This work was supported by National Key Research and Development Program under Grant 2021YFB3800200.

References

[1] Sytnikov VE, Vysotsky VS, Radchenko IP, et al. 1G versus 2G-comparison from the practical standpoint for HTS power cables use. J Phys: Conf Series IOP Publ 2008; 97(1):012058.
[2] Hazelton DW, Selvamanickam V. SuperPower's YBCO coated high-temperature superconducting (HTS) wire and magnet applications. Proc IEEE 2009;97(11): 1831–6.
[3] Senatore C, Alessandrini M, Lucarelli A, Tediosi R, Uglietti D, Iwasa Y. Progresses and challenges in the development of high-field solenoidal magnets based on RE123 coated conductors. Supercond Sci Technol 2014;27(10):103001. https://doi.org/10.1088/0953-2048/27/10/103001.
[4] Shin H-S, Dedicatoria MJ. Intrinsic strain effect on critical current in Cu-stabilized GdBCO coated conductor tapes with different substrates. Supercond Sci Technol 2013;26(5):055005. https://doi.org/10.1088/0953-2048/26/5/055005.
[5] Polikarpova MV, Lukyanov PA, Abdyukhanov IM, et al. Bending strain effects on the critical current in Cu and Cu–Nb–stabilized YBCO-coated conductor tape. IEEE Trans Appl Supercond 2013;24(3):6600604.
[6] Sutoh Y, Kakimoto K, Kaneko N, Iijima Y, Saitoh T. Mechanical bending property of YBCO coated conductor by IBAD/PLD. Physica C (Amsterdam, Neth) 2005;426-431:933–7.
[7] van der Laan DC, Ekin JW. Dependence of the critical current of $YBa_2Cu_3O_{7-\delta}$ coated conductors on in-plane bending. Supercond Sci Technol 2008;21(11): 115002. https://doi.org/10.1088/0953-2048/21/11/115002.
[8] Shin H-S, Dizon JRC, Kim T-H, Ha D-W, Oh S-S. Critical current degradation behavior in YBCO coated conductors under torsional strain. IEEE Trans Appl Supercond 2007;17(2):3274–7.
[9] Wang B, Wu X, Xie H, Lv Z, Wang Z, Song M, et al. Design, Manufacture, and Test of a 30 m 10 kV/2.5 kA Concentric HTS Cable Prototype for Urban Grid. IEEE Access 2021;9:120066–77.
[10] Ilin K, Yagotintsev KA, Zhou C, Gao P, Kosse J, Otten SJ, et al. Experiments and FE modeling of stress–strain state in ReBCO tape under tensile, torsional and transverse load. Supercond Sci Technol 2015;28(5):055006. https://doi.org/10.1088/0953-2048/28/5/055006.
[11] Gao P, Chan W-K, Wang X, Zhou Y, Schwartz J. Stress, strain and electromechanical analyses of (RE) Ba2Cu3Ox conductors using three-dimensional/two-dimensional mixed-dimensional modeling: fabrication, cooling and tensile behavior. Supercond Sci Technol 2020;33(4):044015. https://doi.org/10.1088/1361-6668/ab7778.
[12] De Leon MB, Shin HS. Reliability Evaluation Procedure of Electromechanical Properties in GdBCO CC Tapes Obtained by Uniaxial Tension and Fatigue Tests at 77 K. IEEE Trans Appl Supercond 2020;30(4):9001305.
[13] He R, Tan Y, Huang Z, Xie Y, Wang G, Wang Y, et al. Bending and uniaxial tensile strain effects on the critical current of REBCO coated conductor tapes. Cryogenics 2021;116:103285. https://doi.org/10.1016/j.cryogenics.2021.103285.
[14] Anvar VA, Ilin K, Yagotintsev KA, Monachan B, Ashok KB, Kortman BA, et al. Bending of CORC® cables and wires: finite element parametric study and experimental validation. Supercond Sci Technol 2018;31(11):115006. https://doi.org/10.1088/1361-6668/aadcb9.
[15] Gorospe A, Bautista Z, Shin H-S. Critical current degradation behaviour of GdBCO CC tapes in pure torsion and combined tension-torsion modes. Supercond Sci Technol 2016;29(10):104003. https://doi.org/10.1088/0953-2048/29/10/104003.
[16] Kim HS, Kwon NY, Chang KS, et al. Joint characteristics of the YBCO coated conductor (CC) by chemical etching. IEEE Trans Appl Superconduct 2009; 19(3): 2835–2838.
[17] Song H, Hunte F, Schwartz J. On the role of pre-existing defects and magnetic flux avalanches in the degradation of $YBa_2Cu_3O_{7-x}$ coated conductors by quenching. Acta Mater 2012;60(20):6991–7000.
[18] Rogers S, Chan WK, Schwartz J. Effects of room-temperature tensile fatigue on critical current and n-value of IBAD–MOCVD $YBa_2Cu_3O_{7-x}$/Hastelloy coated conductor. Supercond Sci Technol 2016;29(8):085013. https://doi.org/10.1088/0953-2048/29/8/085013.
[19] Hsueh CH, Paranthaman M. Analytical modeling of residual stresses in multilayered superconductor systems. J Mater Sci 2008;43(18):6223–32.
[20] Xu Y, Chen G, Feng T, Cai Z, Yue Yi, Ren Li, et al. Experimental Study on the Performance Change of YBCO Tapes Under Repeated Overcurrent. IEEE Trans Appl Supercond 2020;30(5):1–10.
[21] Takayasu M, Chiesa L, Bromberg L, Minervini JV. HTS twisted stacked-tape cable conductor. Supercond Sci Technol 2012;25(1):014011. https://doi.org/10.1088/0953-2048/25/1/014011.